Multi-State Energy Landscape for Photoreaction of Stilbene and Dimethyl-stilbene

Takuro Tsutsumi,[a,b] Yuriko Ono,[c] and Tetsuya Taketsugu[a,c]

[a] Department of Chemistry, Faculty of Science, Hokkaido University, Sapporo 060-0810, Japan

[b] L-Station, Creative Research Institution (CRI), Hokkaido University, Sapporo 060-0812, Japan

[c] Institute for Chemical Reaction Design and Discovery (WPI-ICReDD), Hokkaido University, Sapporo 001-0021, Japan

*Corresponding author: Tetsuya Taketsugu

Email: take@sci.hokudai.ac.jp

Keywords: Dimensionality Reduction, Excited State Dynamics, Energy Landscape, Photochemistry, Stilbene

Abstract

We have recently developed the Reaction Space Projector (ReSPer) method, which constructs a reduced-dimensionality reaction space uniquely determined from reference reaction paths for a polyatomic molecular system and projects classical trajectories into the same reaction space. In this paper, we extend ReSPer to the analysis of photoreaction dynamics and relaxation processes of stilbene and present a concept of a "multi-state energy landscape," incorporating the ground- and excited-state reaction subspaces. The multi-state energy landscape successfully explained the previously-established photoreaction processes of *cis*-stilbene, such as the *cis-trans* photoisomerization and the photocyclization. In addition, we discuss the difference in the excited-state reaction dynamics between stilbene and 1,1'-dimethyl-stilbene based on a common reaction subspace determined from a framework part of reference structures with a different number of atoms. This approach allows us to target any molecule with a common framework, greatly expanding the applicability of the ReSPer analysis. The multi-state energy landscape provides fruitful insight into photochemical reactions exploring the excited and ground-state potential energy surfaces, as well as comprehensive reaction processes with non-radiative transitions between adiabatic states, within the stage of a reduced-dimensionality reaction space.

1. Introduction

Recent theoretical studies of photochemical reactions have discussed the lifetimes of products and reaction mechanisms on the basis of the excited-state potential energy surface (PES) and the intersection region of two or more adiabatic PESs. The conical intersection (CI) that intersects adiabatic PESs with the same spin symmetry is now widely recognized as significant for understanding a non-radiative decay process.[1–4] For elucidating the photoreaction mechanisms, it is necessary to explore a series of reaction paths from the Franck-Condon (FC) structure to the CI regions. Various methods so far have been established to obtain the minimum energy CI (MECI) points and the intersection seam, involved in the two-adiabatic PESs.[5–11]

The photoreaction process begins with the initial photoexcitation, where the molecular system transitions from the equilibrium structure of the ground state PES to the excited state PES with a potential gradient, so the effects of reaction dynamics beyond the static reaction pathway picture need to be taken into account in the discussion. On-the-fly molecular dynamics (MD) is a classical trajectory method that does not require a pre-prepared potential function and provides a dynamical trajectory for a given molecular system on a PES determined by electronic structure calculations, taking atomic momentum into account.[12,13] On-the-fly MD has been extended to excited-state reaction dynamics with a surface hopping scheme,[14–19] utilizing Tully's fewest switches algorithm[20] and the Zhu-Nakamura formula for nonadiabatic transitions.[21,22] Since on-the-fly trajectories are time-series data that include all degrees-of-freedom motions of a molecular system, it is difficult to obtain an intuitive picture of what kind of molecular structural changes are taking place from trajectories for complex molecular systems due to their multidimensional nature. Currently, reaction dynamics is discussed by selecting a set of internal coordinates that are considered important in describing the structural changes and projecting the dynamic trajectories onto a subspace consisting of these internal coordinates.

In quantum chemistry, the intrinsic reaction coordinate (IRC),[23,24] defined as the steepest descent path in the mass-weighted coordinate from the first-order saddle point (transition state: TS) toward the reactant minimum or product minimum on the PES, has been used as the reference reaction path in describing elementary processes in chemical

reactions. A reaction path Hamiltonian that takes into account the vibrational degrees of freedom orthogonal to the reaction path along the IRC has also been formulated,[25] and the coupling of reaction coordinates and vibrational coordinates due to reaction-path curvature has been discussed.[25–28] Analyzing on-the-fly trajectories based on a single IRC has also revealed the deviation of the dynamical trajectory in the direction of the curvature vector of the IRC.[27] However, the dynamical trajectory is not necessarily bound to a single IRC; many IRCs form a network on the PES. So far, automated reaction path search methods without prior knowledge of a given molecular system have been established, enabling us to generate the reaction path network.[29–34] Recently, Tsutsumi *et al.* proposed an on-the-fly trajectory mapping method that analyzes dynamical trajectories based on the reaction path network containing multiple IRCs, and found IRC-jump behavior that determines the destination of trajectories in regions where multiple IRCs are in nearby.[35]

The reaction route map and the on-the-fly trajectory are both founded on the full-dimensional PES. Therefore, projecting both of them onto an appropriate subspace that reflects the full-dimensional configurational space makes it possible to visualize dynamical reaction behaviors into a chemical reaction space in the reduced dimension. However, the choice of these coordinates is not unique and requires prior knowledge of the reaction system. In informatics, such ambiguity in coordinate selection can be resolved by dimensionality reduction techniques for extracting data features from high-dimensional data space. Several studies so far have clarified chemical reaction mechanisms using dimensionality reduction techniques, such as the principal component analysis (PCA),[36–38] the multidimensional scaling (MDS),[39–46] the locally linear embedding (LLE),[47] and the isometric feature mapping (Isomap).[40,47]

The classical MDS (CMDS) method provides principal coordinates (PCos) that reproduce the similarity of a given high-dimensional data in a low-dimensional space as much as possible.[48] Therefore, for application to molecular structure data, a relative position of each structure visualized in the subspace by PCos should reproduce their mutual distance relationship in the full-dimensional coordinate space. In 2008, Trosset *et al.* proposed a way for projecting "*out-of-sample*" data into a subspace of lower dimensionality defined by CMDS.[49] Recently, we have developed the *Reaction Space Projector* (*ReSPer*) method that automatically constructs the low-dimensional reaction space and projects on-the-fly trajectories onto the same space using CMDS and the out-

of-sample technique, respectively.[41–44] ReSPer analysis has successfully elucidated dynamical reaction behaviors in the reduced-dimensionality reaction space for several reaction systems, such as the collision reaction of $OH^- + CH_3F \rightarrow [CH_3OH\cdots F]^-$[42,43] and the isomerization and bifurcation reactions of a small gold cluster;[42–44] however, the applications are so far limited to the ground state reactions.

Here, we extend the ReSPer method to photochemical reactions proceeding on PESs in both excited and ground states. As a demonstration of the method, we apply it to the photoreaction of *cis*-stilbene (SB), a well-known photoswitching basic molecule. The ππ* excited *cis*-SB undergoes the photocyclization leading to 4a,4b-dihydrophenanthrene (DHP) and the *cis-trans* photoisomerization relaxing from the *twist* region in the S_1 state,[50–53] where the torsion angle is approximately 90 degrees. Many researchers have devoted considerable effort to elucidating the photoreaction mechanism for *cis*-SB[50–72] and concluded that the dominant reaction process was photoisomerization rather than photocyclization. On the other hand, interestingly, Berndt *et al.* observed that the transient absorption spectra of 1,1'-dimethyl-*cis*-stilbene (*cis*-dmSB), with two methyl groups at the ethylenic part of SB,[73] suggesting that the tendency of photoreaction of *cis*-dmSB in the $S_1(\pi\pi^*)$ state was opposite to that of *cis*-SB. In order to clarify inherent factors for differences between *cis*-SB and *cis*-dmSB, Harabuchi *et al.* investigated the photoreaction mechanisms for both systems by projecting dynamical trajectories onto a two-dimensional subspace defined by two internal coordinates: the C=C torsion angle and the interatomic distance of two carbon atoms involved in photocyclization.[70,74] Subsequently, Tsutsumi *et al.* also studied the photochemistry of α-methyl-*cis*-stilbene[75] and discussed the excited-state branching reaction mechanism in comparison with both *cis*-SB[70] and *cis*-dmSB.[74]

In this study, we define a reduced-dimensionality "multi-state" reaction space determined from reference structures on both S_0- and S_1-state PESs by the ReSPer method. We also incorporate the concept of the energy landscape, which represents the morphology of a single PES, including multiple reaction paths.[45,76–78] In the following, we name the multiple energy landscape generated by adding the axis of potential energy to the principal coordinate axes, constituting the reaction space of multi-electron states, determined by the ReSPer method as the "multi-state energy landscape," and discuss the relaxation process of ππ* excited cis-SB based on the multi-state energy landscape. Furthermore, to clarify the difference between the excited-state PES of SB and dmSB, we

construct a reaction space determined from the dataset of the frame part common to both and compare them to discuss the similarities and differences in the reaction path network.

2. Reaction Space Projector Method

The *Reaction Space Projector* (*ReSPer*) scheme is straightforward: 1) preprocess the structural data of a given molecular system to generate the data required for the dimensionality reduction method, 2) perform the dimensionality reduction to obtain appropriate principal coordinates, 3) (if necessary) project the structural data along the on-the-fly trajectory as out-of-sample data onto the reduced-dimensionality reaction subspace. As the dimensionality reduction method, we use the classical multidimensional scaling (CMDS) method and its out-of-sample extension.[41–44]

2.1. Classical Multidimensional Scaling and Out-of-sample Extension

The CMDS method determines the principal coordinates (PCos) representing the location of each structure based on the distance matrix **D**, whose *ij*th component is the Euclidean distance d_{ij} between structures *i* and *j*. We define the Euclidean distance d_{ij} as the linear distance in 3*N*-dimensional mass-weighted Cartesian coordinates:

$$\mathbf{D}_{ij} = d_{ij} = \sqrt{\sum_{k}^{3N} \left(\xi_k^{(i)} - \xi_k^{(j)}\right)^2} = \left|\boldsymbol{\xi}^{(i)} - \boldsymbol{\xi}^{(j)}\right|, \tag{1}$$

where $\boldsymbol{\xi}^{(i)}$ is the mass-weighted Cartesian coordinate of the *i*th structure of an *N* atomic molecule. The preprocessing process to get the proper pairwise distance between two structures is outlined in the next subsection. The CMDS procedure is as follows: 1) Get the inner matrix **Q** by applying the Young-Householder transformation[79] to the squared distance matrix $\mathbf{D}_{ij}^{(2)} = d_{ij}^2$; 2) Diagonalize **Q** to obtain the eigenvalues $\{\lambda_1, \dots, \lambda_n\}$ and corresponding eigenvectors $\{\mathbf{L}_1, \dots, \mathbf{L}_n\}$, where *n* is the total number of refence structures; 3) Select the *p* largest eigenvalues and corresponding eigenvectors to generate *p* principal coordinates (PCos), $\mathbf{X}_a = \mathbf{L}_a\sqrt{\lambda_a}$ $(1 \le a \le p)$. Since the eigenvalue λ_a means the amount of information of the *a*th principal coordinate, we can verify the availability of dimensionality reduction by the proportion of eigenvalues:[48]

$$\Lambda_a = \frac{\lambda_a}{\sum_c^b \lambda_c}, \tag{2}$$

$$\Lambda = \sum_c^p \Lambda_c = \frac{\sum_c^p \lambda_c}{\sum_c^b \lambda_c}, \tag{3}$$

where *b* is the total number of positive eigenvalues. These are referred to as the proportion of variance Λ_a and the cumulated proportion Λ, respectively.

Embedding new data into a reduced-dimensionality subspace is accomplished by the out-of-sample technique. Trosset formulated the out-of-sample extension of the CMDS method,[49] and we implemented this procedure in the ReSPer program to project an on-the-fly trajectory data into the low-dimensional reaction space determined by CMDS. The CMDS method and the out-of-sample embedding procedure are summarized in the literature.[41–44,48,49]

2.2. Preprocessing of Molecular Structures

In order to construct a reasonable reaction space, the orientation of reference structures needs to be aligned before running the ReSPer program. This is because it greatly affects the accuracy of the distance matrix. For a given pair of structures, the center of mass must be fixed at the coordinate origin, and the x-y-z coordinate axes must be rotated so that the distance between the structures is minimized. The latter axes rotation is conducted by the Kabsch algorithm.[80,81] However, even after the molecular structure alignment, the appropriate distance may not necessarily be obtained if the order of the identical atoms is switched. Molecules in which the order of identical atoms is switched are called nuclear-permutation inversion (NPI) isomers to the original structure, and the structural distance (eq 1) between the two NPI isomers is greater than zero, even though the molecular structures are identical. For the NPI problem, we so far devised a merged-NPI procedure that assigns the smallest distance between all NPI isomers of each structure as the pairwise distance d_{ij} when determining the distance between structure *i* and structure *j*.[35]

Although the merged-NPI procedure can search for the most suitable NPI isomers for a given reference structure, generating a distance matrix involving numerous NPI

isomers is not practical. For example, in the case of stilbene ($C_{14}H_{12}$), the total number of NPI isomers is $14! \times 12! \times 2 \approx 8.4 \times 10^{19}$. In practice, it is unnecessary to consider structural changes such as the exchange of two atoms in a chemically stable part (e.g., benzene ring) or between distant parts because these changes raise the energy barrier. Therefore, in this study, only 16 (= $2^2 \times 2 \times 2$) NPI isomers generated by internal rotation of two phenyl groups, inversion operation, and atom-map flipping were selected as NPI isomers to be considered in the merged-NPI method. Atom-map flipping is an operation that flips the numbering of the atoms of a stilbene molecule (or a stilbene derivative) with respect to the central C=C bond. Here, we would like to emphasize the difference between the inversion operation and the atom-map flipping. As shown in **Figure 1**, S_1-MIN_{twist} has a pyramidal shape around C2 with the C2-Ph group rotating to the front side of the paper; when the inversion operation is performed on S_1-MIN_{twist}, the C2-Ph group rotates to the back side of the paper, producing a chiral isomer with a pyramidal shape around C2. In contrast, in the atom-map flipping, the NPI isomer has the C1-Ph group rotated to the back side of the paper, producing a pyramidal shape around C1.

3. Computational Details

Referring to the previous reports on SB[70] and dmSB,[74] several minimum structures (MIN), TS structures, and MECI structures were determined by exploring the PES in the S_0 and S_1 states for SB and dmSB. To obtain the connectivity of each structure in the S_0 and S_1 states, we calculated the IRC[23,24] from the TS structure and the meta-IRC (= the steepest descent path starting from a non-stationary point) from the three Franck-Condon (FC) structures on the S_1 state and from the three MECI structures. Note that the three MECIs found in this study are not peaked CIs located as minima on the PES in the excited state but sloped CIs,[82] so one meta-IRC on each PES for each MECI was obtained. All electronic structure calculations were performed by the spin-flip time-dependent density functional theory (SF-TDDFT)[83] method with BHHLYP functional and 6-31G* basis set, using the GAMESS program.[84] The geometry optimization and the reaction path calculation were conducted by the GRRM17 program[85], in which the gradient projection method was employed in the MECI optimizations, with the state-tracking method.[70,74] We further carried out normal mode analysis to verify the features of TSs. The Cartesian

coordinates of MIN, TS, and MECI structures for SB and dmSB discussed in this article are given in Supporting Information.

We also performed on-the-fly MD simulations for *cis*-SB on the PESs in the S_1 and S_0 states to comprehensively discuss the dynamics of non-radiative decay at the same SF-TDDFT level by the SPPR program[86] combined with the GAMESS program.[84] The time evolution of Newton's equation of motion was conducted by the velocity-Verlet algorithm. We also used the state-tracking method proposed in the previous study[70,74] to track the target state of interest (see **Figure S1** in SI). First, on-the-fly MD simulations were performed for ππ*-excited *cis*-SB on the S_1-PES, with initial conditions determined by normal-mode sampling of S_0-MIN_{cis}: the atomic coordinates and velocities were generated by adding the initial energy to each normal mode according to the Boltzmann distribution at 300 K. The time step was set to 0.2 fs, and 22 trajectories were run until the energy difference between the S_0 and S_1 states was less than 0.2 eV (~ 4.6 kcal/mol). After reaching the CI region, the trajectories were hopped to the S_0-PES, and the MD simulation was continued in the ground state for 1 ps. For *cis*-dmSB, we analyzed on-the-fly trajectories that were previously reported.[74] The Cartesian coordinates for initial, hopping, and terminal points of on-the-fly trajectories discussed in this article are given in Supporting Information.

In principle, the ReSPer program can handle a large number of molecular structures comprising reaction paths and on-the-fly trajectories, but it is time-consuming and the reaction space becomes cumbersome. Therefore, we thinned down the number of structures to about 10 for each forward-IRC, backward-IRC, and meta-IRC. For on-the-fly trajectories, only structures with local potential minima along time were selected as reference structures.

The accuracy of electronic structure calculations for SB has been discussed in various sophisticated methods.[54,71,72,87] Ioffe *et al.* performed the extended multiconfiguration quasi-degenerate perturbation theory (XMCQDPT2) calculations for SB on the S_0 and S_1 states and reported that the SF-TDDFT results were not quantitative, but the feature of S_1-PES was qualitatively consistent with XMCQDPT2.[71] The validations for SF-TDDFT compared with the sophisticated methods[71,87] are summarized in **Table S1** (see SI). Moreover, the non-adiabatic dynamics simulations of the excited *cis*-SB have shown good

agreement with experimentally observed lifetime and branching ratio.[55–58] It is noted that our interest is to extend the ReSPer analysis to the multi-state energy landscape, and therefore, we focus on how dynamical reaction processes are represented in the multi-state landscape rather than statistical aspects of the destinations of trajectories.

4. Results and Discussion

4.1. Ground-state Energy Landscape for Stilbene

Figure 1 shows the molecular structures of SB and their relative energies in the S_0 and S_1 states, which were calculated in this study. Hereafter, S_i-MIN_A, S_i-$TS_{A\text{-}B}$, and S_i/S_j-$MECI_A$ denote the MIN structure of the A form in the S_i state, the TS structure connecting the A and B forms in the S_i state, and the MECI structure in the A region between the S_i and S_j states. Note that the structure form (region) A includes *cis*, *trans*, DHP, and *twist*. We also calculated relevant IRCs and meta-IRCs.

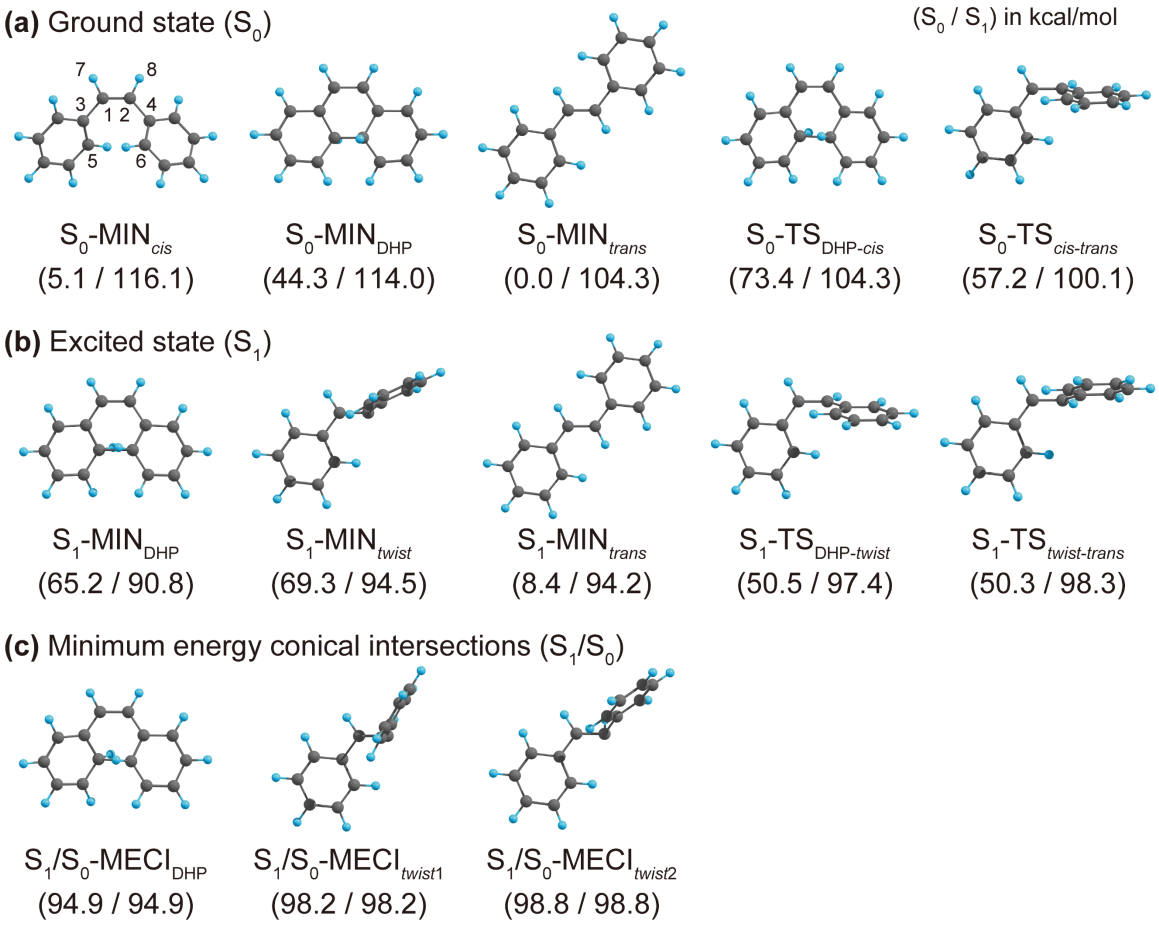

Figure 1. Molecular structures for stilbene. (a) Three minima (MIN) and two transition state (TS) structures in the S_0 state, **(b)** three MIN and two TS structures in the S_1 state, and **(c)** three minimum energy conical intersection (MECI) structures between the S_0 and S_1 states. S_i-MIN_A, S_i-$TS_{A\text{-}B}$, and S_i/S_j-$MECI_A$ denote the MIN structure of the A form in the S_i state, the TS structure connecting the A and B forms in the S_i state, and the MECI structure in the A region between the S_i and S_j states. Note that the structure form (region) A includes *cis*, *trans*, DHP, and *twist*. The different MECIs in the *twist* region are distinguished as S_1/S_0-$MECI_{twist1}$ and S_1/S_0-$MECI_{twist2}$ in order to decrease potential energy. The potential energies relative to S_0-MIN_{trans} are shown as (S_0 energy / S_1 energy) in kcal/mol.

Figure 2a shows the reaction route map in the two-dimensional reaction space determined by applying ReSPer to 79 reference structures including three S_0-MIN, two S_0-

TS, three S_1/S_0-MECI, as well as structures on two IRCs and three meta-IRCs, for the ground state of SB. For simplicity, the molecular structures along each reaction path are not depicted, but these structures were used in the ReSPer analysis. The (Λ_1, Λ_2), which represents the proportion of the variance of PCo1 and PCo2, is (0.882, 0.054), and the cumulated proportion is 0.936, confirming that the two PCos almost completely describe the reaction space of the ground state of SB. The other proportions are summarized in **Fig. S2a** (see SI). As shown in Fig. 2, PCo1 well describes the structural change along the part of the IRC starting from S_0-$TS_{cis\text{-}trans}$, which correlates with the torsion motion of the central C=C bond leading to *cis-trans* isomerization. PCo2 changes along the IRC from S_0-$TS_{DHP\text{-}cis}$ to S_0-MIN_{DHP} and along the meta-IRC starting from S_1/S_0-$MECI_{twist1}$ and S_1/S_0-$MECI_{twist2}$. As PCo2 decreases, the C5-C3-C1-C2-C4-C6 moiety (the ethylene moiety and two phenyl groups; atom numbering is shown in Fig.1) flattens out regardless of the direction of each phenyl group. Indeed, as shown in Fig. 1, the C5-C3-C1-C2-C4-C6 chains are pseudo-orthogonal in S_1/S_0-$MECI_{twist1}$ and S_1/S_0-$MECI_{twist2}$ with large PCo2, and their chains are pseudo-parallel in S_0-MIN_{DHP} and S_0-MIN_{trans} with small PCo2. These structural changes suggest the difficulty of representing PCo2 in terms of simple internal coordinates.

Photoreaction mechanisms of SB and its derivatives have been discussed based on a two-dimensional coordinate space in terms of the dihedral angle of the central part and the C5-C6 interatomic distance, which characterize *cis-trans* isomerization and cyclization reactions, respectively.[70,74,75] However, these two coordinates are strongly correlated, as indicated by the increase in the interatomic distance with increasing the dihedral angle. This feature supports that the two elementary processes under study are approximately reproduced by a single reaction coordinate of PCo1, as seen in the proportion of the variance of PCo1. Indeed, an examination of the variation of the internal coordinates along PCo1 confirms a positive correlation between the dihedral angle of the central part and the C5-C6 interatomic distance, as shown in **Fig. S3a** (see SI).

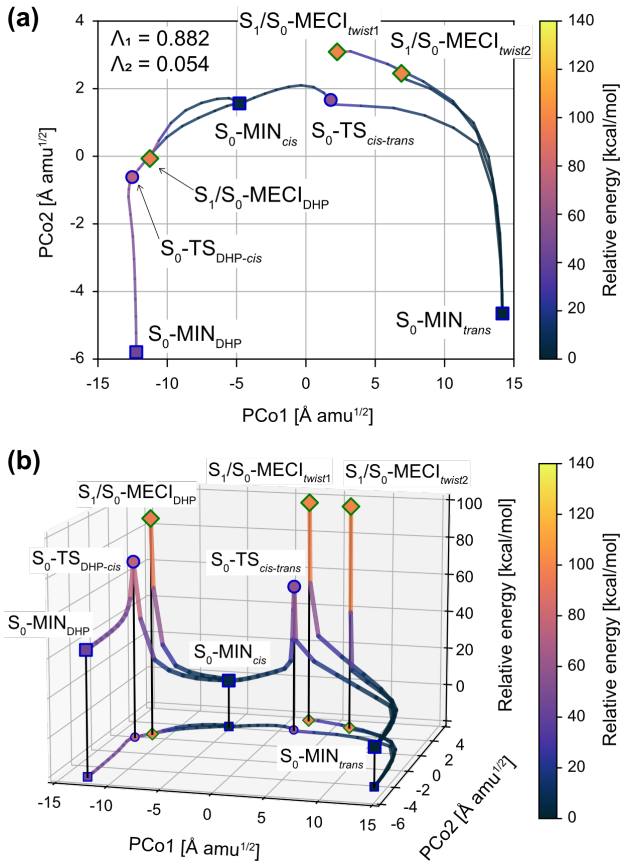

Figure 2. Ground-state reaction route map and energy landscape for stilbene determined from the reference structures in S_0-PES. (a) Two-dimensional reaction space defined by principal coordinates (PCos) and **(b)** energy landscape and its projection onto the PCo1-PCo2 plane. Three S_0-MINs, two S_0-TSs, and three S_1/S_0-MECIs are shown as squares, circles, and diamonds, respectively. Five reaction paths, including two IRCs from S_0-TSs and three meta-IRCs from S_1/S_0-MECIs, are represented by a single line. The marker edge color indicates on which PES the molecular structure was optimized: blue for S_0-PES and green for the crossing point between S_1-PES and S_0-PES. The proportion of the variance of PCo1 and PCo2, (Λ_1, Λ_2), is shown in (a). The potential energy value is indicated by the color map with respect to S_0-MIN$_{trans}$.

Adding the information of potential energy to the grids in the reduced-dimensionality reaction space provides an intuitive understanding of the shape of PES. Figure 2b shows the ground-state energy landscape with the relative potential energy in

the S_0 state as the third axis. It is noted that the visualized IRC profile appears to descend sharply from S_0-TS on the energy landscape due to data thinning. Comparing the barrier heights of S_0-$TS_{DHP\text{-}cis}$ (73.4 kcal/mol) and S_0-$TS_{cis\text{-}trans}$ (57.2 kcal/mol), as discussed below, *cis*-SB on the ground-state energy landscape thermodynamically prefers *cis*-*trans* isomerization to cyclization to DHP-form, but either reaction can energetically occur through relaxation from S_1/S_0-MECIs to the ground state in each region.

Figure 2 also contains three meta-IRCs originating from three S_1/S_0-MECIs corresponding to the sloped CIs. The meta-IRC starting from S_1/S_0-$MECI_{DHP}$ reaches S_0-MIN_{cis} because the meta-IRC merges at the *cis* side when it joins the IRC connecting S_0-MIN_{DHP} and S_0-MIN_{cis} in the S_0 state. For the same reason, meta-IRCs starting from S_1/S_0-$MECI_{twist1}$ and S_1/S_0-$MECI_{twist2}$ proceed on S_0-PES towards *trans*-region and finally reach S_0-MIN_{trans}.

4.2. Excited-state Energy Landscape for Stilbene

Next, we construct the excited-state two-dimensional reaction route map for SB by ReSPer, including three S_1-MINs, two S_1-TSs, three S_1/S_0-MECIs, and eight reaction paths on S_1-PES, for a total of 111 structures (**Fig. 3a**). Note that three S_0-MINs are also included as Franck-Condon (FC) structures on S_1-PES. Figure 3b shows the excited-state energy landscape corresponding to Fig. 3a. The proportion of variance (Λ_1, Λ_2) is (0.860, 0.085), indicating that two PCos sufficiently reproduce the excited-state reaction route map for SB. Other proportions are summarized in **Fig. S2b** (see SI). Interestingly, the physical meaning of PCo1 and PCo2 coincide well with those of the ground-state reaction route map (Fig. 2). Note that, in the excited-state landscape, the pyramidalization angle correlates somewhat more with PCo2 than in the ground-state landscape, as shown in **Fig. S3b** (see SI). This result suggests that the reduced-dimensionality reaction route maps of the ground and excited states can be determined together by common principle coordinates without significant influence on their relative configuration.

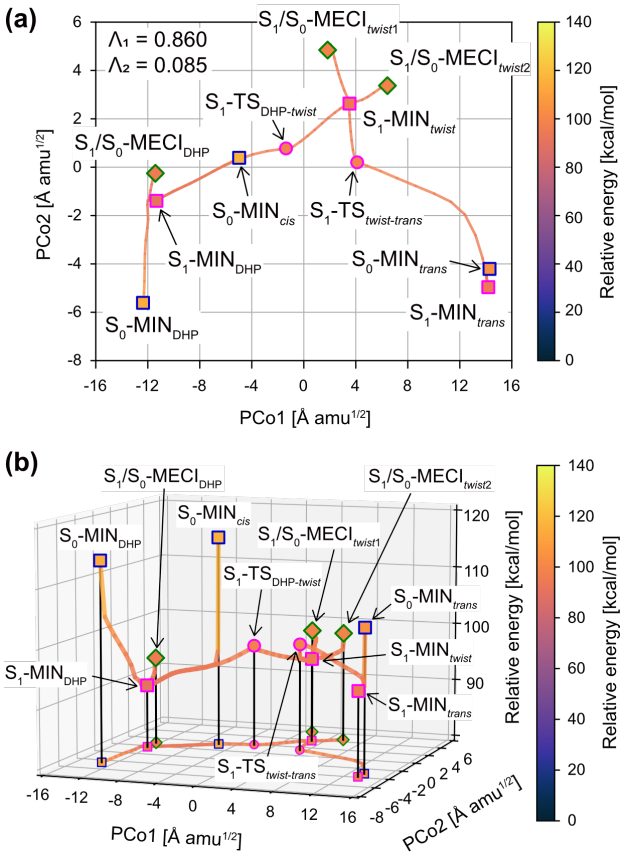

Figure 3. Excited-state reaction route map and energy landscape for stilbene determined from the reference structures on S_1-PES. (a) Two-dimensional reaction space defined by principal coordinates (PCos) and **(b)** energy landscape and its projection onto the PCo1-PCo2 plane. Six minima (S_0-MINs and S_1-MINs), two S_1-TSs, and three S_1/S_0-MECIs are denoted by squares, circles, and diamonds, respectively. Eight reaction paths, including two IRCs from S_1-TSs, three meta-IRCs from the Franck-Condon structures of S_0-MINs, and three meta-IRCs from S_1/S_0-MECIs, are denoted by a single line. The marker edge color indicates on which PES the molecular structure was optimized: blue for S_0-PES, pink for S_1-PES, and green for the crossing point between S_1- and S_0-PESs, respectively. The proportion of the variance of PCo1 and PCo2, (Λ_1, Λ_2), is shown in (a). The potential energy value is indicated by the color map with respect to S_0-MIN$_{trans}$.

As shown in Fig. 3b, the meta-IRC from the FC structure of S_0-MIN_{cis} on the S_1-PES immediately merges into the IRC between S_1-$TS_{DHP\text{-}twist}$ and S_1-MIN_{DHP}, with a sharp energy decrease. Figure 3b also intuitively shows that the excited *cis*-SB can dynamically access all S_1/S_0 crossing regions because the potential energy of the FC structure at S_0-MIN_{cis} is relatively higher than at S_1/S_0-MECIs. In addition, as discussed in previous studies,[70] meta-IRC from S_1/S_0-$MECI_{DHP}$ reaches S_1-MIN_{DHP} directly without energy barriers, and meta-IRCs from S_1/S_0-$MECI_{twist1}$ or S_1/S_0-$MECI_{twist2}$ reach S_1-MIN_{twist} without energy barriers. Thus, the reduced-dimensionality energy landscape highlights the relationship between the shape of the reaction route network and the excited state reaction dynamics on S_1-PES.

Many experimental efforts have been devoted to elucidating the relaxation processes of *cis*- and *trans*-SB from a common *twist* region to the ground state, especially the existence of barriers from each FC structure to the *twist* region.[50–52,59–63] For *cis*-SB, it is recognized that the ππ*-excited molecule proceeds to the *twist* region with almost no barrier on the excited-state PES, which is supported by the ultrafast relaxation to the ground state within 2.0 ps.[51,59] Harabuchi *et al.* theoretically demonstrated that excited *cis*-SB preferred a conformational change to the *twist*-form and smoothly relaxed to the ground state through the conical intersection in the *twist* region.[70] Based on these results and the excited-state energy landscape in Fig. 3b, the experimentally suggested small barriers may correspond to the reaction barrier with S_1-$TS_{DHP\text{-}twist}$ (6.6 kcal/mol from S_1-MIN_{DHP} to S_1-MIN_{twist}) or the energy difference between S_1-MIN_{twist} and two MECIs (S_1/S_0-$MECI_{twist1}$ and S_1/S_0-$MECI_{twist2}$). On the other hand, since *trans*-SB has a relatively long lifetime of 25 ps[61] than *cis*-SB, it is experimentally confirmed that there is a planar stable structure near the FC region and that a small barrier along the reaction path from the planar structure to the *twist* region exists.[62,63] In the reduced-dimensionality reaction space, the planar minimum structure, S_1-MIN_{trans}, is located near the FC structure of S_0-MIN_{trans}, indicating that a potential barrier of 4.1 kcal/mol is required for *trans*-*twist* isomerization *via* S_1-$TS_{twist\text{-}trans}$. This result supports the morphology of S_1-PES with a reaction barrier of 1200 cm^{-1} (~ 3.4 kcal/mol) reported in previous studies.[62,63]

4.3. Multi-state Energy Landscape for Stilbene

To reveal a comprehensive photoreaction path based on both ground and excited states, we construct the "*multi-state*" reaction route map and energy landscape by ReSPer. **Figure 4a** shows the multi-state reaction space containing 228 structures in total, including six minima, four TSs, three S_1/S_0-MECIs, and 13 reaction paths. Note that each S_0-MIN has two data points, the minimum structure on the S_0-PES and the FC point on the S_1-PES, which overlap in Fig. 4a. The multi-state energy landscape corresponding to Fig. 4a is also shown in Fig. 4b. The proportion of variances (Λ_1, Λ_2) is (0.865, 0.069), and the relative locations of molecular structures in each state are similar to the respective single-state reaction route maps. Other proportions are summarized in **Fig. S2c** (see SI). These results indicate that, as expected in the above section, the two PCos adequately reproduce the multi-state reaction space and have almost the same meanings as Figs. 2 and 3.

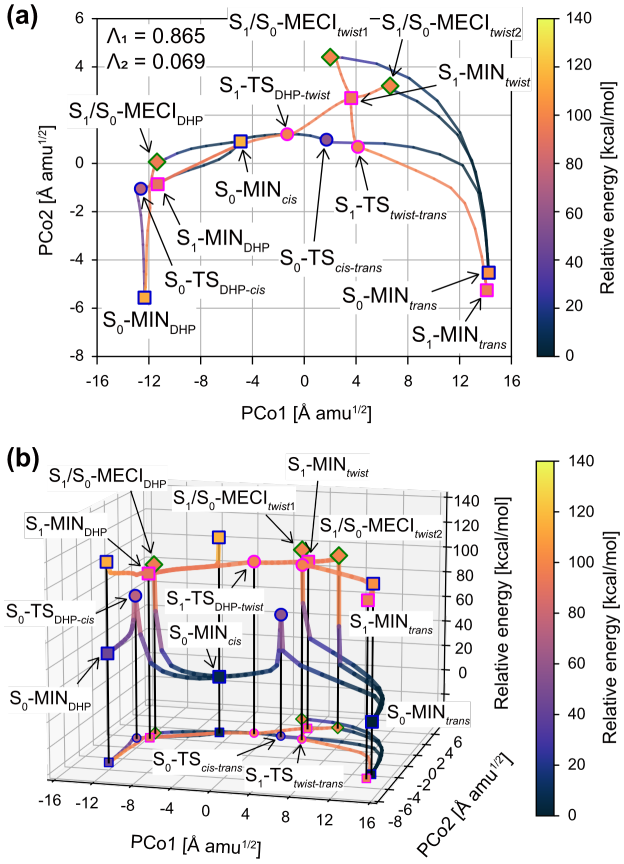

Figure 4. Multi-state reaction route map and energy landscape for stilbene determined from the reference structures on both S_0- and S_1-PESs. (a) Two-dimensional reaction space defined by principal coordinates (PCos) and **(b)** energy landscape and its projection onto the PCo1-PCo2 plane. Six minima (S_0-MINs and S_1-MINs), four TSs (S_0-TSs and S_1-TSs), and three S_1/S_0-MECIs are denoted by squares, circles, and diamonds, respectively. Thirteen reaction paths, including four IRCs and nine meta-IRCs, are indicated by a single line. Note that each S_0-MIN has two data points, the minimum structure on the S_0-PES and the Franck-Condon point on the S_1-PES, which overlap in Fig. 4a. The marker edge color indicates on which PES the molecular structure was optimized: blue for S_0-PES, pink for S_1-PES, and green for the crossing point of S_1-PES and S_0-PES. The proportion of the variance of PCo1 and PCo2, (Λ_1, Λ_2), is shown in (a). The potential energy value is indicated by the color map with respect to S_0-MIN_{trans}.

The *cis*-*trans* photoisomerization of SB has traditionally been discussed on the basis of a one-dimensional potential energy curve with a dihedral angle around the central ethylene part. Along this potential energy curve, the S_0-PES has a large barrier around the approximately 90° twisted region, whereas the S_1-PES stabilizes in the same twisted region, where the S_0 and S_1 states are considered to be degenerate. Therefore, ππ*-excited *cis*-SB is recognized to decay through the twisted region and finally relax to the *trans*- or *cis*-form in the S_0 state.[50–53] However, in general, the choice of internal coordinates to describe a reaction process requires chemical intuition, and no one can guarantee their appropriateness for discussing chemical reactions.

The reduced-dimensionality reaction route map constructed by ReSPer is mathematically guaranteed to reproduce the position of the molecular structure in the full-dimensional space as much as possible in the low-dimensional space. Consequently, the dimensionality reduction map and its energy landscape are very useful tools for describing chemical reaction processes. The two-dimensional reaction space in Fig. 4a indicates that the *cis*-*trans* photoisomerization reaction occurs as PCo1 increases; around PCo1 = 0 ~ 4 Å $amu^{1/2}$, the potential energy of the S_1 state decreases while the potential energy of the S_0 state increases. Focusing on PCo1, which accounts for 86.3% of the positional information on the reference structures, S_0-$TS_{cis\text{-}trans}$ is located very close to S_1-MIN_{twist}, as

assumed in the conventional one-dimensional scheme. However, the multi-state energy landscape in Fig. 4b shows that the energy difference between the S_1 and S_0 states becomes zero at S_1/S_0-MECI$_{twist1}$ and S_1/S_0-MECI$_{twist2}$ rather than near S_0-TS$_{cis\text{-}trans}$ and S_1-MIN$_{twist}$, which are separated from the twisted MECIs by PCo2. This picture has been reported from sophisticated electronic structure calculations,[71] indicating that the non-radiative relaxation to the ground state should be discussed in the two-dimensional reaction space. On the other hand, S_0-TS$_{DHP\text{-}cis}$ and S_1-MIN$_{DHP}$ are close to each other in the two-dimensional reaction space and their energies are also close, which is due to the rigidity of the DHP form. Thus, the reduced-dimensionality reaction space and energy landscape provide useful insights into the morphology of PES that cannot be captured from conventional reaction schemes.

4.4. On-the-fly Trajectory Analysis based on Multi-state Energy Landscape for Stilbene

Next, we discuss the non-radiative decay mechanisms of *cis*-SB on S_1- and S_0-PESs based on the reduced-dimensionality reaction route map. **Figure 5** shows two on-the-fly trajectories projected by the out-of-sample technique[42,49] into the multi-state reaction space shown in Fig. 4a. Figures 5e-f show the projection of these two trajectories onto the multi-state energy landscape shown in Fig. 4b.

Figures 5a-b show the on-the-fly trajectory relaxing from the S_1-DHP region to the ground state: the reaction processes on S_1-PES and S_0-PES are shown in Fig. 5a and Fig. 5b, respectively. Figure 5e shows the same trajectory projected into the multi-state energy landscape. After ππ* excitation around the S_0-MIN$_{cis}$ structure, this trajectory initially goes toward the *twist* region on S_1-PES, approaching S_1/S_0-MECI$_{twist2}$, but it does not reach the CI region and goes to the DHP region *via* the S_1-TS$_{DHP\text{-}twist}$. It then relaxes to S_0-PES in a region around S_1/S_0-MECI$_{DHP}$ and finally gets trapped in the S_0-DHP region without crossing the S_0-TS$_{DHP\text{-}cis}$. Interestingly, although some trajectories hopped to the ground state on the *cis* side of the IRC going through S_0-TS$_{DHP\text{-}cis}$, all trajectories relaxing from the S_1-DHP region were trapped in the S_0-DHP region in the ground state. This result suggests that after relaxing from the S_1-DHP region, the photoreaction process prefers to undergo photocyclization with the velocity direction maintained on S_1-PES and then trapped in the

S_0-DHP region. The relaxed trajectory has much higher energy than the potential energy on the reaction path in the ground state, but in order to cross the S_0-$TS_{DHP\text{-}cis}$ in the ground state, this excess energy must be converted to the direction of the reaction coordinate.

Figures 5c-d show the case of on-the-fly trajectory relaxing from the *twist* region to the ground state: the reaction processes on S_1-PES and S_0-PES are shown in Fig. 5c and Fig. 5d, respectively. Figure 5f shows the same trajectory projected into the multi-state energy landscape. This trajectory first goes toward the S_1-DHP region following the meta-IRC from the FC point of S_0-MIN_{cis}, but goes to the *twist* region and enters the CI region around S_1/S_0-$MECI_{twist1}$. After relaxation to S_0-PES, it initially goes to the *cis* region and then moves to the *trans* region, but returns to the *cis* region. In contrast to Fig. 5b, this trajectory entering the *trans* region on S_0-PES comes back easily to the *cis* region because of the lower energy barrier of S_0-$TS_{cis\text{-}trans}$ than that of S_0-$TS_{DHP\text{-}cis}$, as shown in the energy landscape of Fig. 5f. Of course, each trajectory has sufficiently higher energy than S_0-TSs. The nature of the decay process and the fact that excited *cis*-SB prefers photoisomerization to the *twist*-form on S_1-PES[51,59,60] support the fact that the *cis*-form is the dominant product after the molecule relaxes to the ground state.[64–66] The ReSPer analysis can reveal comprehensive photochemical reaction processes based on the multi-state energy landscape that serves as the stage for chemical reactions.

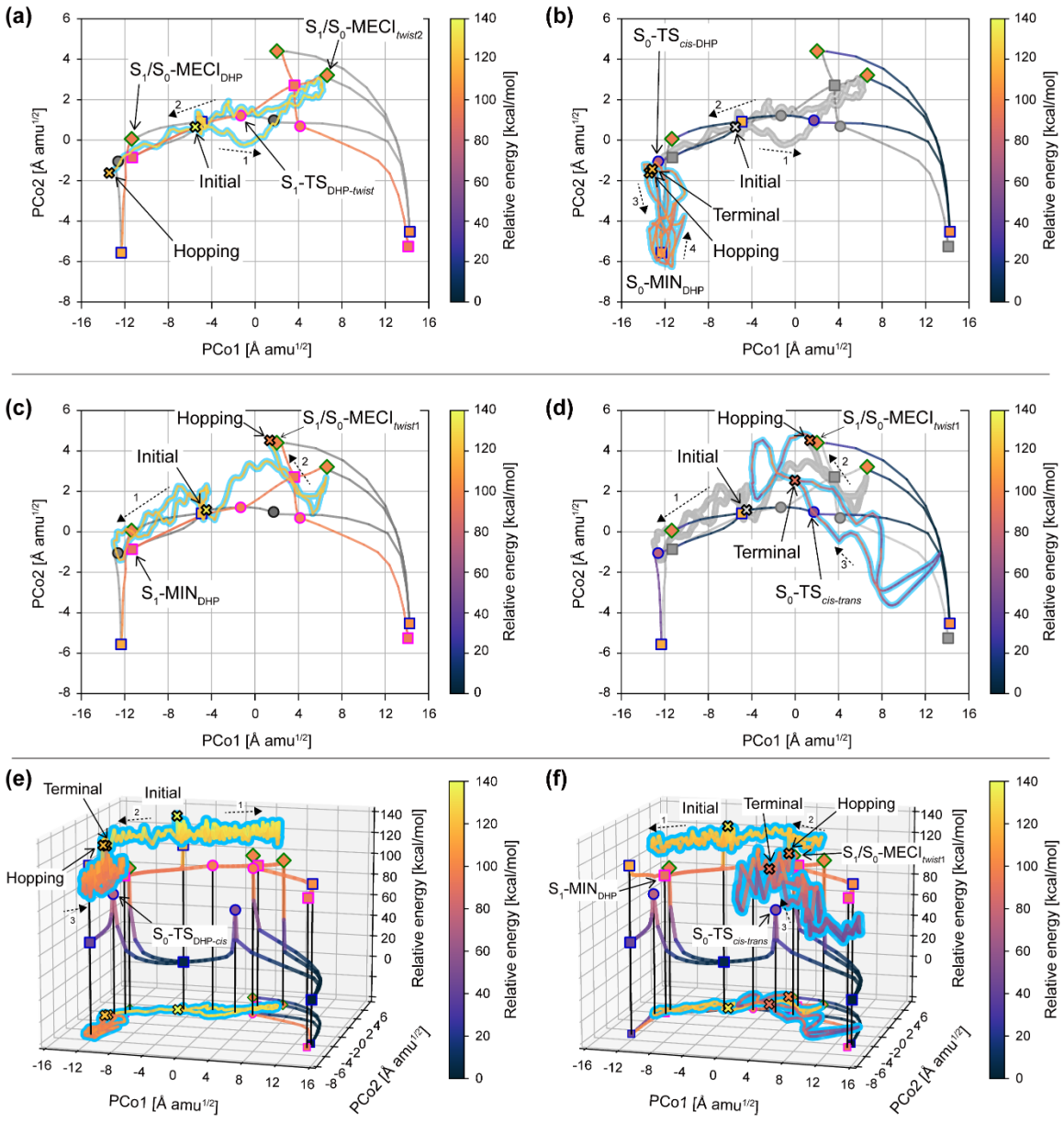

Figure 5. On-the-fly trajectories projected onto the two-dimensional multi-state reaction space and energy landscape predefined in Figs. 4a and 4b, respectively. On-the-fly trajectory **(a)** which proceeds from S_0-MIN_{cis} to S_1/S_0-$MECI_{DHP}$ *via* the *twist* region on S_1-PES and **(b)** gets trapped around S_0-MIN_{DHP} after hopping to S_0-PES from the S_1/S_0-$MECI_{DHP}$ region. On-the-fly trajectory **(c)** which proceeds from S_0-MIN_{cis} to S_1/S_0-$MECI_{twist1}$ *via* the DHP region on S_1-PES and **(d)** approaches S_0-MIN_{cis} after hopping to S_0-PES from the S_1/S_0-$MECI_{twist1}$ region. **(e-f)** Overall picture of projected trajectories on the multi-state energy landscape. The trajectories are indicated by blue lines, while the

"initial" point, the "hopping" point from S_1-PES to S_0-PES, and the "terminal" point of each trajectory are denoted by cross marks. The time evolution of each trajectory is shown by the dashed arrows with the numbers representing the time order. The color map and the third axis in Fig.5d show the potential energy relative to S_0-MIN_{trans} for both the reaction route map and the on-the-fly trajectories.

The relevance of ReSPer analysis and non-adiabatic dynamics simulations for photoreactions should also be mentioned. With the surface hopping MD scheme[20] and the *ab initio* multiple spawning method,[88] ab initio non-adiabatic dynamics simulations have become the standard approach for studying comprehensive photoreaction mechanisms, and stilbene, a benchmark molecule for photoisomerization reactions, has been thoroughly investigated.[55–58] Since the only information required for ReSPer analysis is molecular structure data, it is straightforward to apply ReSPer to classical trajectory-based non-adiabatic MD approaches. Several automated approaches have been presented that systematically search for minimum energy crossing points[9] and intersection seam[10,11] according to the topology of two adiabatic PES, allowing the discovery of complex photochemical reaction processes without prior knowledge. The latter uses meta-dynamics to efficiently sample seam regions, depending on the definition of the collective variables. In the future, we plan to apply the ReSPer method to provide representative reaction coordinates as collective variables.

4.5. Reaction Space Analysis for Stilbene and Dimethyl-stilbene

Finally, differences in excited-state reaction dynamics between *cis*-stilbene (SB) and 1,1'-dimethyl-*cis*-stilbene (dmSB) were examined based on a common reduced-dimensionality reaction space. Previous studies have compared these photoreaction mechanisms based on a common subspace determined by two internal coordinates.[70,74] Such dimensionality reduction is feasible for molecular systems with different numbers of atoms, but requires chemical intuition for the proper choice of internal coordinates. On the other hand, the ReSPer approach using the CMDS method provides a unique principal coordinate for determining the reduced dimension, but the definition of the Euclidean distance limits its application to molecular systems with the same number of atoms.

To overcome this problem, we focused on the common part of SB and dmSB. In this study, we defined the $C_{14}H_{10}$ part consisting of the central C=C part and two phenyl groups as the framework, and generated a reduced-dimensionality reaction space determined from the $C_{14}H_{10}$ framework structure with seven minima: S_0-MIN$_{cis}$, S_1-MIN$_{DHP}$, and S_1-MIN$_{twist}$ for SB and dmSB, and S_1-MIN$_{cis}$ for dmSB only. **Figure 6a** shows the excited-state reaction space determined by the framework structures of the seven minima for SB and dmSB, with a cumulated proportion of 0.969. As shown in Fig. 6a, the structural changes along PCo1 are mainly related to isomerization between DHP and *twist* forms on S_1-PES, while PCo2 clearly disperses the FC points (S_0-MIN$_{cis}$) of SB and dmSB. It is noteworthy that only dmSB has a *cis*-form in the S_1 state that is close to the S_0-MIN$_{cis}$ of SB.

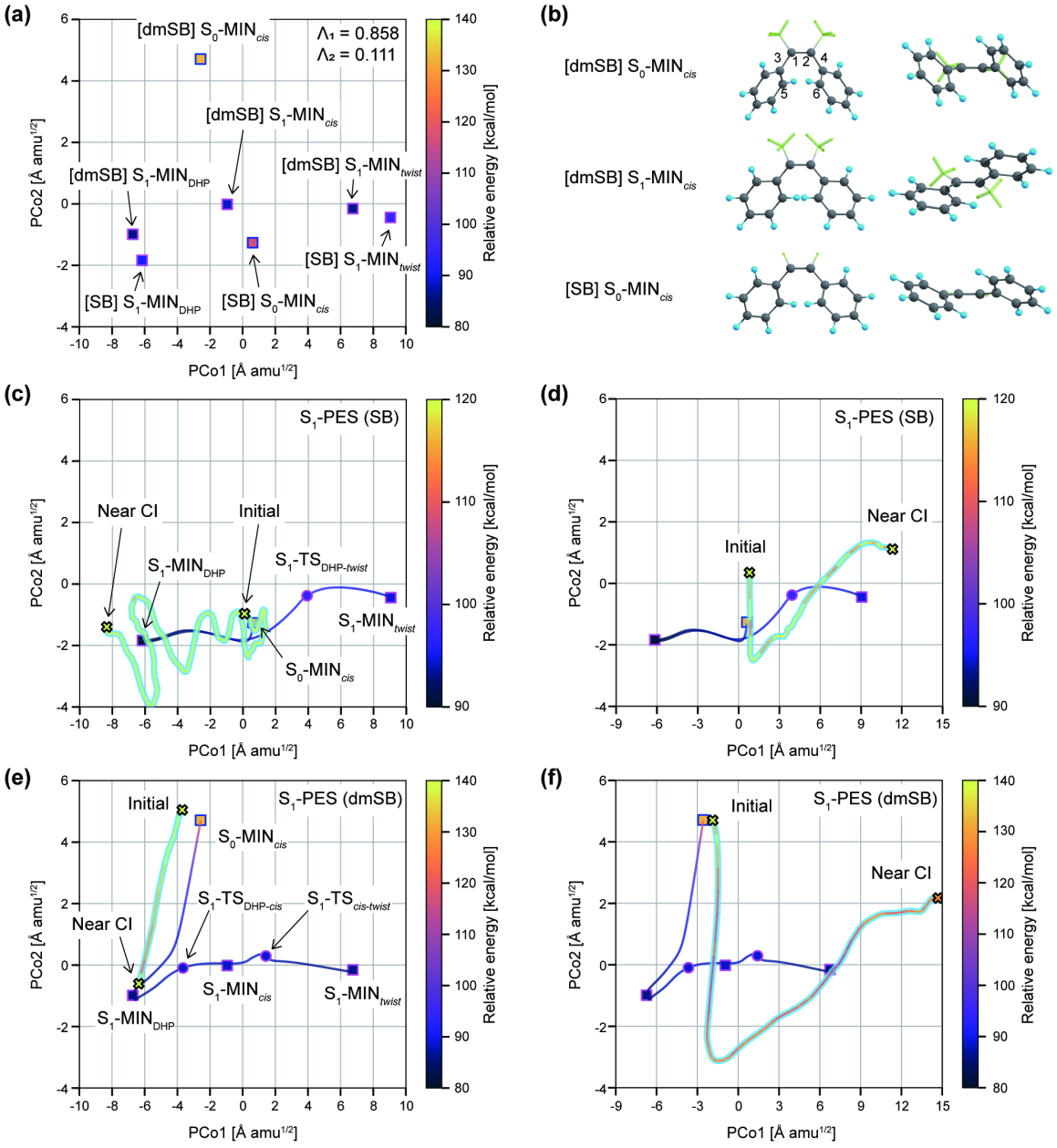

Figure 6. Two-dimensional excited-state reaction space determined from the common framework parts of the reference structures for stilbene (SB) and 1,1'-dimethyl-stilbene (dmSB) and the on-the-fly trajectories projected onto the common excited-state reaction space. (a) Two-dimensional excited-state reaction space determined from the common framework part of the seven minima of SB and dmSB. **(b)** Three molecular structures of the *cis*-form distributed by PCo2 in Fig. 6a. Non-common parts are shown in light green. **(c-d)** Typical trajectories of SB toward S_1-MIN_{DHP} and S_1-

MIN_{twist}, respectively. **(e-f)** Typical trajectories of dmSB toward S_1-MIN_{DHP} and S_1-MIN_{twist}, respectively. Note that in (c-f), only the corresponding reference structures are plotted. Trajectories are indicated by blue lines, and initial points and the vicinity of the CI (denoted Near CI) are indicated by crosses. The color maps show the potential energy with respect to S_0-MIN_{trans} for both the reaction route map and the on-the-fly trajectories, where the ranges are suitable for the reference structures.

The differences between the three *cis*-form structures (S_0-MIN_{cis} of SB and S_0-MIN_{cis} and S_1-MIN_{cis} of dmSB) distributed in the PCo2 direction help us better understand the differences between the excited-state PES of SB and dmSB. Figure 6b shows these three *cis*-form structures from two different directions. The major difference between the S_0-MIN_{cis} of SB and dmSB is the relative orientation of the two phenyl groups: in SB, they are oriented nearly parallel to the plane consisting of C3-C1-C2-C4, while in dmSB, they are not. In the S_1-MIN_{cis} of dmSB, this orientation is similar to that of the S_0-MIN_{cis} of SB, supporting the relative positions of the three *cis*-form structures shown in Fig. 6a. In previous studies, a common two-dimensional subspace was defined by the two internal coordinates summarized in **Table 1**, and differences in excited-state reaction dynamics were discussed.[70,74] However, the structural differences between the S_0-MIN_{cis} of SB and the S_0-MIN_{cis} of dmSB, which correspond to FC points on the S_1-PES, could not be described due to insufficient description by internal coordinates. The advantage of the ReSPer analysis is that it provides a flexible understanding of the structural features of different molecular systems by extracting the principal coordinates determined from the distance matrices associated with the partial framework structures.

Table 1. Principal coordinates PCos (in Å $amu^{1/2}$), C5-C6 interatomic distances r_{C5C6} (in Å), and C3-C1-C2-C4 torsion angles $d_{C3C1C2C4}$ (in degrees) for the seven original structures shown in Fig. 6a. The numbering of the atoms is shown in Fig. 6b.

	PCo1	PCo2	r_{C5C6}	$d_{C3C1C2C4}$
[dmSB] S_1-MIN_{DHP}	-6.73	-0.99	2.06	17.06
[SB] S_1-MIN_{DHP}	-6.16	-1.84	2.09	17.88

[dmSB] S_0-MIN$_{cis}$	-2.58	4.71	3.42	8.20
[dmSB] S_1-MIN$_{cis}$	-0.94	-0.02	2.93	50.82
[SB] S_0-MIN$_{cis}$	0.61	-1.27	3.21	7.30
[dmSB] S_1-MIN$_{twist}$	6.75	-0.15	3.84	103.12
[SB] S_1-MIN$_{twist}$	9.05	-0.45	4.14	112.83

To compare the excited-state dynamics of *cis*-SB and *cis*-dmSB, the reaction paths and on-the-fly trajectories were projected onto a common reaction subspace (Fig. 6a) using out-of-sample techniques.[42,49] Figures 6c and 6d show the reduced-dimensionality excited-state reaction subspace of *cis*-SB and two typical trajectories proceeding to the DHP and *twist* regions. Similarly, Figs. 6e and 6f are for *cis*-dmSB. Note that the reaction paths and on-the-fly trajectories are embedded in a two-dimensional subspace predefined by the seven original structures shown in Fig. 6a, and only the corresponding original structures are plotted in Figs. 6c-f. It has been reported that in the early stages of excited-state dynamics, *cis*-SB takes longer to form DHP-SB because the rapid rotation around the C=C bond stimulates molecular vibrations perpendicular to the direction of C-C bond formation.[70] Figures 6c and 6d show well the trend of the excited-state dynamics of *cis*-SB. On the other hand, it has been reported that *cis*-dmSB prefers to form a new C-C bond to become a DHP-form rather than to become a twist-form by rotation around the C=C bond.[74] From the ReSPer results in Figs. 6e and 6f, the initial dynamic behavior of *cis*-dmSB after ππ* excitation is expected to reorient the two phenyl rings along the meta-IRC from the FC structure of S_0-MIN$_{cis}$, strongly correlated with the PCo2 change. This trend supports the predominance of DHP-form formation. In order to form the twist-form, it is necessary to cross the vicinity of the S_1-MIN$_{cis}$, with an opening already at the two phenyl groups, away from the meta-IRC. From the above discussion, it is clear that even different molecular systems can be compared in terms of PES morphology and reaction dynamics by constructing a common reaction subspace based on the partial framework structure.

5. Conclusion

Cis-stilbene is known to undergo both *cis-trans* photoisomerization and photocyclization after ππ* excitation, and the mechanism of relaxation from the excited state to the ground state is of great experimental and theoretical interest. The excited-state dynamics of *cis*-stilbene and its derivatives have been discussed based on a projection onto a two-dimensional reaction subspace defined by two internal coordinates that characterize the structural changes to each product. However, this two-dimensional subspace is not unique, since the choice of internal coordinates depends on chemical intuition. To avoid such ambiguity, we applied the *Reaction Space Projector* (*ReSPer*) method to construct a reduced-dimensionality reaction route map defined by mathematically selected principal coordinates by means of the classical multidimensional scaling (CMDS) method, one of the dimensionality reduction methods.

The two-dimensional reaction space of the ground and excited states constructed by ReSPer was a good representation of the *cis-trans* photoisomerization and photocyclization reactions. Each principal coordinate was correlated with the torsional angle around the central C=C bond, as well as with the structural flatness of the ethylene moiety and the two phenyl groups. For a comprehensive analysis of the photochemical reaction process, a multi-state reaction space was constructed from the data set of ground and excited-state molecular structures and reaction paths. As a useful concept, a multi-state energy landscape was presented by adding a third axis of relative potential energy to the two-dimensional multi-state reaction subspace, and dynamic reaction routes including non-radiative decay were discussed based on the multi-state energy landscape. These results indicate that the ReSPer analysis provides comprehensive chemical insight into photochemical reaction processes based on the morphology of the potential energy surface in both excited and ground states.

To compare the differences in excited-state reaction dynamics between stilbene (SB) and 1,1'-dimethylstilbene (dmSB), the excited-state reaction space was defined by a partial framework structure common to SB and dmSB. In this study, $C_{14}H_{10}$, consisting of a central C=C part and two phenyl groups, was selected as the framework part. By defining the reaction subspace in this way, it became possible to embed different molecular systems in the same coordinate space. These analyses revealed that the Franck-Condon point of *cis*-dmSB differs significantly from that of *cis*-SB, although the other reference structures of dmSB are located near the reference structure of SB on the two-dimensional

common reaction space. The morphological features in these excited states were qualitatively consistent with the trends in excited state dynamics.

ReSPer analysis successfully constructs not only single-state reduced-dimensionally reaction spaces, but also multi-state reaction spaces without prior knowledge of the chemical reaction under investigation. Multi-state analysis provides a comprehensive strategy for investigating the dynamics of complex photochemical reactions based on ground and excited-state PES. The multi-state energy landscape, which includes reaction paths, especially meta-IRCs of both ground and excited states, reveals the correspondence between the morphology of PES and the behavior of chemical reaction dynamics. The ReSPer method will be useful in elucidating photochemical reaction mechanisms that are sensitively controlled by the multi-state PES morphology.

Acknowledgments

T. Tsutsumi was financially supported by Wakeshima Makoto Research Fellowship. This work was partly supported by the Photo-excitonix Project in Hokkaido University, JST CREST Grant Number JPMJCR1902, and JSPS KAKENHI Grant Number JP22K14640. A part of calculations was performed using Research Center for Computational Science, Okazaki, Japan (Project: 22-IMS-C019).

Author Contributions

The manuscript was written through contributions of all authors.

Competing Interests

The authors declare no competing interests.

ORCID

Takuro Tsutsumi: 0000-0001-5086-1122

Tetsuya Taketsugu: 0000-0002-1337-6694

Supporting Information.

Validations of spin-flip TDDFT compared with the high-accuracy methods (Figure S1 and Table S1), the proportion of variances for S_0-, S_1-, and multi-state PESs (Figure S2), changes in internal coordinates along principal coordinates determined by ReSPer (Figure S3), and the Cartesian coordinates of significant molecular structures of stilbene and 1,1'-dimethyl stilbene (Section IV and V).

References

(1) Sobolewski, A. L.; Domcke, W.; Dedonder-Lardeux, C.; Jouvet, C. Excited-State Hydrogen Detachment and Hydrogen Transfer Driven by Repulsive 1πσ* States: A New Paradigm for Nonradiative Decay in Aromatic Biomolecules. *Phys. Chem. Chem. Phys.* **2002**, *4*, 1093–1100.

(2) Domcke, W.; Stock, G. Theory of Ultrafast Nonadiabatic Excited-State Processes and Their Spectroscopic Detection in Real Time. In *Advances in Chemical Physics*; Prigogine, I., Rice, S. A., Eds.; 2007; Vol. 100, pp 1–169.

(3) Domcke, W.; Yarkony, D. R. Role of Conical Intersections in Molecular Spectroscopy and Photoinduced Chemical Dynamics. *Annu. Rev. Phys. Chem.* **2012**, *63*, 325–352.

(4) Karsili, T. N. V.; Marchetti, B.; Ashfold, M. N. R.; Domcke, W. Ab Initio Study of Potential Ultrafast Internal Conversion Routes in Oxybenzone, Caffeic Acid, and Ferulic Acid: Implications for Sunscreens. *J. Phys. Chem. A* **2014**, *118*, 11999–12010.

(5) Koga, N.; Morokuma, K. Determination of the Lowest Energy Point on the Crossing Seam between Two Potential Surfaces Using the Energy Gradient. *Chem. Phys. Lett.* **1985**, *119*, 371–374.

(6) Bearpark, M. J.; Robb, M. A.; Bernhard Schlegel, H. A Direct Method for the Location of the Lowest Energy Point on a Potential Surface Crossing. *Chem. Phys. Lett.* **1994**, *223*, 269–274.

(7) Maeda, S.; Ohno, K.; Morokuma, K. Automated Global Mapping of Minimal Energy Points on Seams of Crossing by the Anharmonic Downward Distortion Following Method: A Case Study of H 2 CO. *J. Phys. Chem. A* **2009**, *113*, 1704–1710.

(8) Quapp, W.; Bofill, J. M.; Caballero, M. Search for Conical Intersection Points (CI) by Newton Trajectories. *Chem. Phys. Lett.* **2012**, *541*, 122–127.

(9) Maeda, S.; Harabuchi, Y.; Taketsugu, T.; Morokuma, K. Systematic Exploration of Minimum Energy Conical Intersection Structures near the Franck–Condon Region. *J. Phys. Chem. A* **2014**, *118*, 12050–12058.

(10) Lindner, J. O.; Sultangaleeva, K.; Röhr, M. I. S.; Mitrić, R. MetaFALCON: A Program Package for Automatic Sampling of Conical Intersection Seams Using Multistate Metadynamics. *J. Chem. Theory Comput.* **2019**, *15*, 3450–3460.

(11) Pieri, E.; Lahana, D.; Chang, A. M.; Aldaz, C. R.; Thompson, K. C.; Martínez, T. J. The Non-Adiabatic Nanoreactor: Towards the Automated Discovery of Photochemistry. *Chem. Sci.* **2021**, *12*, 7294–7307.

(12) Gordon, M. S.; Chaban, G.; Taketsugu, T. Interfacing Electronic Structure Theory with Dynamics. *J. Phys. Chem.* **1996**, *100*, 11512–11525.

(13) Pratihar, S.; Ma, X.; Homayoon, Z.; Barnes, G. L.; Hase, W. L. Direct Chemical Dynamics Simulations. *J. Am. Chem. Soc.* **2017**, *139*, 3570–3590.

(14) Taketsugu, T.; Tajima, A.; Ishii, K.; Hirano, T. Ab Initio Direct Trajectory Simulation with Nonadiabatic Transitions of the Dissociative Recombination Reaction HCNH + + e − → HNC/HCN + H . *Astrophys. J.* **2004**, *608*, 323–329.

(15) Ootani, Y.; Satoh, K.; Nakayama, A.; Noro, T.; Taketsugu, T. Ab Initio Molecular Dynamics Simulation of Photoisomerization in Azobenzene in the Nπ* State. *J. Chem. Phys.* **2009**, *131*, 194306.

(16) Nanbu, S.; Ishida, T.; Nakamura, H. Future Perspectives of Nonadiabatic Chemical Dynamics. *Chem. Sci.* **2010**, *1*, 663.

(17) Kamiya, M.; Taketsugu, T. Ab Initio Surface Hopping Excited‐state Molecular Dynamics Approach on the Basis of Spin–Orbit Coupled States: An Application to the A‐band Photodissociation of CH 3 I. *J. Comput. Chem.* **2019**, *40*, 456–463.

(18) Yu, L.; Xu, C.; Lei, Y.; Zhu, C.; Wen, Z. Trajectory-Based Nonadiabatic Molecular Dynamics without Calculating Nonadiabatic Coupling in the Avoided Crossing Case: Trans ↔ Cis Photoisomerization in Azobenzene. *Phys. Chem. Chem. Phys.* **2014**, *16*, 25883–25895.

(19) Kanno, M.; Ito, Y.; Shimakura, N.; Koseki, S.; Kono, H.; Fujimura, Y. Ab Initio Quantum Dynamical Analysis of Ultrafast Nonradiative Transitions via Conical Intersections in Pyrazine. *Phys. Chem. Chem. Phys.* **2015**, *17*, 2012–2024.

(20) Tully, J. C. Molecular Dynamics with Electronic Transitions. *J. Chem. Phys.* **1990**, *93*, 1061–1071.

(21) Zhu, C.; Nakamura, H. The Two‐state Linear Curve Crossing Problems Revisited. II. Analytical Approximations for the Stokes Constant and Scattering Matrix: The Landau–Zener Case. *J. Chem. Phys.* **1992**, *97*, 8497–8514.

(22) Zhu, C.; Nakamura, H. The Two‐state Linear Curve Crossing Problems Revisited. III. Analytical Approximations for Stokes Constant and Scattering Matrix: Nonadiabatic Tunneling Case. *J. Chem. Phys.* **1993**, *98*, 6208–6222.

(23) Fukui, K. A Formulation of the Reaction Coordinate. *J. Phys. Chem.* **1970**, *74*, 4161.

(24) Maeda, S.; Harabuchi, Y.; Ono, Y.; Taketsugu, T.; Morokuma, K. Intrinsic Reaction Coordinate: Calculation, Bifurcation, and Automated Search. *Int. J. Quantum Chem.* **2015**, *115*, 258–269.

(25) Miller, W. H.; Handy, N. C.; Adams, J. E. Reaction Path Hamiltonian for Polyatomic Molecules. *J. Chem. Phys.* **1980**, *72*, 99–112.

(26) Kato, S.; Morokuma, K. Potential Energy Characteristics and Energy Partitioning in Chemical Reactions: Ab Initio MO Study of $H_2CCH_2F \rightarrow H_2CCHF+H$ Reaction. *J. Chem. Phys.* **1980**, *72*, 206–217.

(27) Taketsugu, T.; Gordon, M. S. Dynamic Reaction Path Analysis Based on an Intrinsic Reaction Coordinate. *J. Chem. Phys.* **1995**, *103*, 10042–10049.

(28) Konkoli, Z.; Kraka, E.; Cremer, D. Unified Reaction Valley Approach Mechanism of the Reaction CH 3 + H 2 → CH 4 + H. *J. Phys. Chem. A* **1997**, *101*, 1742–1757.

(29) Rappoport, D.; Galvin, C. J.; Zubarev, D. Y.; Aspuru-Guzik, A. Complex Chemical Reaction Networks from Heuristics-Aided Quantum Chemistry. *J. Chem. Theory Comput.* **2014**, *10*, 897–907.

(30) Martínez-Núñez, E. An Automated Method to Find Transition States Using Chemical Dynamics Simulations. *J. Comput. Chem.* **2015**, *36*, 222–234.

(31) Yang, M.; Zou, J.; Wang, G.; Li, S. Automatic Reaction Pathway Search via Combined Molecular Dynamics and Coordinate Driving Method. *J. Phys. Chem. A* **2017**, *121*, 1351–1361.

(32) Dewyer, A. L.; Argüelles, A. J.; Zimmerman, P. M. Methods for Exploring Reaction Space in Molecular Systems. *WIREs Comput. Mol. Sci.* **2018**, *8*, 1–20.

(33) Field-Theodore, T. E.; Taylor, P. R. ALTRUISM: A Higher Calling. *J. Chem. Theory Comput.* **2020**, *16*, 4388–4398.

(34) Maeda, S.; Harabuchi, Y. Exploring Paths of Chemical Transformations in Molecular and Periodic Systems: An Approach Utilizing Force. *WIREs Comput. Mol. Sci.* **2021**, *11*, 1–23.

(35) Tsutsumi, T.; Harabuchi, Y.; Ono, Y.; Maeda, S.; Taketsugu, T. Analyses of Trajectory On-the-Fly Based on the Global Reaction Route Map. *Phys. Chem. Chem. Phys.* **2018**, *20*, 1364–1372.

(36) Komatsuzaki, T.; Hoshino, K.; Matsunaga, Y.; Rylance, G. J.; Johnston, R. L.; Wales, D. J. How Many Dimensions Are Required to Approximate the Potential Energy Landscape of a Model Protein? *J. Chem. Phys.* **2005**, *122*, 084714.

(37) Hare, S. R.; Bratholm, L. A.; Glowacki, D. R.; Carpenter, B. K. Low Dimensional Representations along Intrinsic Reaction Coordinates and Molecular Dynamics Trajectories Using Interatomic Distance Matrices. *Chem. Sci.* **2019**, *10*, 9954–9968.

(38) Peng, J.; Xie, Y.; Hu, D.; Lan, Z. Analysis of Bath Motion in MM-SQC Dynamics via Dimensionality Reduction Approach: Principal Component Analysis. *J. Chem. Phys.* **2021**, *154*, 094122.

(39) Pisani, P.; Caporuscio, F.; Carlino, L.; Rastelli, G. Molecular Dynamics Simulations and Classical Multidimensional Scaling Unveil New Metastable States in the Conformational Landscape of CDK2. *PLoS One* **2016**, *11*, e0154066.

(40) Li, X.; Xie, Y.; Hu, D.; Lan, Z. Analysis of the Geometrical Evolution in On-the-Fly Surface-Hopping Nonadiabatic Dynamics with Machine Learning Dimensionality

Reduction Approaches: Classical Multidimensional Scaling and Isometric Feature Mapping. *J. Chem. Theory Comput.* **2017**, *13*, 4611–4623.

(41) Tsutsumi, T.; Ono, Y.; Arai, Z.; Taketsugu, T. Visualization of the Intrinsic Reaction Coordinate and Global Reaction Route Map by Classical Multidimensional Scaling. *J. Chem. Theory Comput.* **2018**, *14*, 4263–4270.

(42) Tsutsumi, T.; Ono, Y.; Arai, Z.; Taketsugu, T. Visualization of the Dynamics Effect: Projection of on-the-Fly Trajectories to the Subspace Spanned by the Static Reaction Path Network. *J. Chem. Theory Comput.* **2020**, *16*, 4029–4037.

(43) Tsutsumi, T.; Ono, Y.; Taketsugu, T. Visualization of Reaction Route Map and Dynamical Trajectory in Reduced Dimension. *Chem. Commun.* **2021**, *57*, 11734–11750.

(44) Tsutsumi, T.; Ono, Y.; Taketsugu, T. Reaction Space Projector (ReSPer) for Visualizing Dynamic Reaction Routes Based on Reduced-Dimension Space. *Top. Curr. Chem.* **2022**, *380*, 19.

(45) Oliveira Junior, A. B.; Lin, X.; Kulkarni, P.; Onuchic, J. N.; Roy, S.; Leite, V. B. P. Exploring Energy Landscapes of Intrinsically Disordered Proteins: Insights into Functional Mechanisms. *J. Chem. Theory Comput.* **2021**, *17*, 3178–3187.

(46) Oliveira, A. B.; Yang, H.; Whitford, P. C.; Leite, V. B. P. P. Distinguishing Biomolecular Pathways and Metastable States. *J. Chem. Theory Comput.* **2019**, *15*, 6482–6490.

(47) Shi, W.; Jia, T.; Li, A. Quasi-Classical Trajectory Analysis with Isometric Feature Mapping and Locally Linear Embedding: Deep Insights into the Multichannel Reaction on an $NH3^+$ (^4A) Potential Energy Surface. *Phys. Chem. Chem. Phys.* **2020**, *22*, 17460–17471.

(48) Härdle, W. K.; Simar, L. In *Applied Multivariate Statistical Analysis*, 3rd Edit.; Springer Berlin Heidelberg: Berlin, Heidelberg, Heidelberg, 2015.

(49) Trosset, M. W.; Priebe, C. E. The Out-of-Sample Problem for Classical Multidimensional Scaling. *Comput. Stat. Data Anal.* **2008**, *52*, 4635–4642.

(50) Saltiel, J. Perdeuteriostilbene. The Role of Phantom States in the Cis-Trans Photoisomerization of Stilbenes. *J. Am. Chem. Soc.* **1967**, *89*, 1036–1037.

(51) Todd, D. C.; Jean, J. M.; Rosenthal, S. J.; Ruggiero, A. J.; Yang, D.; Fleming, G. R. Fluorescence Upconversion Study of Cis ‐ stilbene Isomerization. *J. Chem. Phys.* **1990**, *93*, 8658–8668.

(52) Fuß, W.; Kosmidis, C.; Schmid, W. E.; Trushin, S. A. The Photochemicalcis–Trans Isomerization of Free Stilbene Molecules Follows a Hula-Twist Pathway. *Angew. Chemie Int. Ed.* **2004**, *43*, 4178–4182.

(53) Nakamura, T.; Takeuchi, S.; Taketsugu, T.; Tahara, T. Femtosecond Fluorescence Study of the Reaction Pathways and Nature of the Reactive S1 State of Cis-Stilbene. *Phys. Chem. Chem. Phys.* **2012**, *14*, 6225.

(54) Tomasello, G.; Garavelli, M.; Orlandi, G. Tracking the Stilbene Photoisomerization in the S1 State Using RASSCF. *Phys. Chem. Chem. Phys.* **2013**, *15*, 19763.

(55) Neukirch, A. J.; Shamberger, L. C.; Abad, E.; Haycock, B. J.; Wang, H.; Ortega, J.; Prezhdo, O. V.; Lewis, J. P. Nonadiabatic Ensemble Simulations of Cis-Stilbene and Cis -Azobenzene Photoisomerization. *J. Chem. Theory Comput.* **2014**, *10*, 14–23.

(56) Liu, Y.; Xia, S. H.; Zhang, Y. Photochemical and Photophysical Properties of Cis-Stilbene Molecule by Electronic Structure Calculations and Nonadiabatic Surface-Hopping Dynamics Simulations. *Chem. Phys.* **2020**, *539*, 110957.

(57) Weir, H.; Williams, M.; Parrish, R. M.; Hohenstein, E. G.; Martínez, T. J. Nonadiabatic Dynamics of Photoexcited Cis -Stilbene Using Ab Initio Multiple Spawning. *J. Phys. Chem. B* **2020**, *124*, 5476–5487.

(58) Williams, M.; Forbes, R.; Weir, H.; Veyrinas, K.; Macdonell, R. J.; Boguslavskiy, A. E.; Schuurman, M. S.; Stolow, A.; Martinez, T. J. Unmasking the Cis-Stilbene Phantom State via Vacuum Ultraviolet Time-Resolved Photoelectron Spectroscopy and Ab Initio Multiple Spawning. *J. Phys. Chem. Lett.* **2021**, *12*, 6363–6369.

(59) Greene, B. I.; Farrow, R. C. Subpicosecond Time Resolved Multiphoton Ionization: Excited State Dynamics of Cis‐stilbene under Collision Free Conditions. *J. Chem. Phys.* **1983**, *78*, 3336–3338.

(60) Kovalenko, S. A.; Dobryakov, A. L.; Ioffe, I.; Ernsting, N. P. Evidence for the Phantom State in Photoinduced Cis–Trans Isomerization of Stilbene. *Chem. Phys. Lett.* **2010**, *493*, 255–258.

(61) Greene, B. I.; Hochstrasser, R. M.; Weisman, R. B. Spectroscopic Study of the Picosecond Photoisomerization of Stilbene. *Chem. Phys. Lett.* **1979**, *62*, 427–430.

(62) Syage, J. A.; Lambert, W. R.; Felker, P. M.; Zewail, A. H.; Hochstrasser, R. M. Picosecond Excitation and TRANS-CIS Isomerization of Stilbene in a Supersonic Jet: Dynamics and Spectra. *Chem. Phys. Lett.* **1982**, *88*, 266–270.

(63) Baskin, J. S.; Bañares, L.; Pedersen, S.; Zewail, A. H. Femtosecond Real-Time Probing of Reactions. 20. Dynamics of Twisting, Alignment, and IVR in the Trans -Stilbene Isomerization Reaction. *J. Phys. Chem.* **1996**, *100*, 11920–11933.

(64) Muszkat, K. A.; Fischer, E. Structure, Spectra, Photochemistry, and Thermal Reactions of the 4a,4b-Dihydrophenanthrenes. *J. Chem. Soc. B Phys. Org.* **1967**, No. 0, 662.

(65) Petek, H.; Yoshihara, K.; Fujiwara, Y.; Lin, Z.; Penn, J. H.; Frederick, J. H. Is the Nonradiative Decay of S1 Cis-Stilbene Due to the Dihydrophenanthrene Isomerization Channel? Suggestive Evidence from Photophysical Measurements on 1,2-Diphenylcycloalkenes. *J. Phys. Chem.* **1990**, *94*, 7539–7543.

(66) Rodier, J. M.; Myers, A. B. Cis-Stilbene Photochemistry: Solvent Dependence of the Initial Dynamics and Quantum Yields. *J. Am. Chem. Soc.* **1993**, *115*, 10791–10795.

(67) Quenneville, J.; Martínez, T. J. Ab Initio Study of Cis−Trans Photoisomerization in Stilbene and Ethylene. *J. Phys. Chem. A* **2003**, *107*, 829–837.

(68) Takeuchi, S.; Ruhman, S.; Tsuneda, T.; Chiba, M.; Taketsugu, T.; Tahara, T. Spectroscopic Tracking of Structural Evolution in Ultrafast Stilbene Photoisomerization. *Science (80-.).* **2008**, *322*, 1073–1077.

(69) Minezawa, N.; Gordon, M. S. Photoisomerization of Stilbene: A Spin-Flip Density Functional Theory Approach. *J. Phys. Chem. A* **2011**, *115*, 7901–7911.

(70) Harabuchi, Y.; Keipert, K.; Zahariev, F.; Taketsugu, T.; Gordon, M. S. Dynamics Simulations with Spin-Flip Time-Dependent Density Functional Theory: Photoisomerization and Photocyclization Mechanisms of Cis- Stilbene in Ππ* States. *J. Phys. Chem. A* **2014**, *118*, 11987–11998.

(71) Ioffe, I. N.; Granovsky, A. A. Photoisomerization of Stilbene: The Detailed XMCQDPT2 Treatment. *J. Chem. Theory Comput.* **2013**, *9*, 4973–4990.

(72) Chaudhuri, R. K.; Freed, K. F.; Chattopadhyay, S.; Mahapatra, U. S. Theoretical Studies of the Ground and Excited State Structures of Stilbene. *J. Phys. Chem. A* **2013**, *117*, 9424–9434.

(73) Berndt, F.; Dobryakov, A. L.; Quick, M.; Mahrwald, R.; Ernsting, N. P.; Lenoir, D.; Kovalenko, S. A. Long-Lived Perpendicular Conformation in the Photoisomerization Path of 1,1′-Dimethylstilbene and 1,1′-Diethylstilbene. *Chem. Phys. Lett.* **2012**, *544*, 39–42.

(74) Harabuchi, Y.; Yamamoto, R.; Maeda, S.; Takeuchi, S.; Tahara, T.; Taketsugu, T. Ab Initio Molecular Dynamics Study of the Photoreaction of 1,1′-Dimethylstilbene upon S 0 → S 1 Excitation. *J. Phys. Chem. A* **2016**, *120*, 8804–8812.

(75) Tsutsumi, T.; Harabuchi, Y.; Yamamoto, R.; Maeda, S.; Taketsugu, T. On-the-Fly Molecular Dynamics Study of the Excited-State Branching Reaction of α-Methyl-Cis-Stilbene. *Chem. Phys.* **2018**, *515*, 564–571.

(76) Wales, D. J.; Doye, J. P. K. Global Optimization by Basin-Hopping and the Lowest Energy Structures of Lennard-Jones Clusters Containing up to 110 Atoms. *J. Phys. Chem. A* **1997**, *101*, 5111–5116.

(77) Wales, D. J.; Miller, M. A.; Walsh, T. R. Archetypal Energy Landscapes. *Nature* **1998**, *394*, 758–760.

(78) Wales, D. In *Energy Landscapes*; Cambridge University Press: Cambridge, 2004.

(79) Young, G.; Householder, A. S. Discussion of a Set of Points in Terms of Their Mutual Distances. *Psychometrika* **1938**, *3*, 19–22.

(80) Kabsch, W. A Solution for the Best Rotation to Relate Two Sets of Vectors. *Acta Crystallogr. Sect. A* **1976**, *32*, 922–923.

(81) Charnley Kromann, J. rmsd. *GitHub*. GitHub repository, http://github.com/charnley/rmsd, (accessed September 14, 2022).

(82) Malhado, J. P.; Hynes, J. T. Photoisomerization for a Model Protonated Schiff Base in Solution: Sloped/Peaked Conical Intersection Perspective. *J. Chem. Phys.* **2012**, *137*.

(83) Shao, Y.; Head-Gordon, M.; Krylov, A. I. The Spin-Flip Approach within Time-Dependent Density Functional Theory: Theory and Applications to Diradicals. *J. Chem. Phys.* **2003**, *118*, 4807–4818.

(84) Schmidt, M. W.; Baldridge, K. K.; Boatz, J. A.; Elbert, S. T.; Gordon, M. S.; Jensen, J. H.; Koseki, S.; Matsunaga, N.; Nguyen, K. A.; Su, S.; Windus, T. L.; Dupuis, M.; Montgomery, J. A. General Atomic and Molecular Electronic Structure System. *J. Comput. Chem.* **1993**, *14*, 1347–1363.

(85) Maeda, S.; Harabuchi, Y.; Takagi, M.; Saita, K.; Suzuki, K.; Ichino, T.; Sumiya, Y.; Sugiyama, K.; Ono, Y. Implementation and Performance of the Artificial Force Induced Reaction Method in the GRRM17 Program. *J. Comput. Chem.* **2018**, *39*, 233–251.

(86) Harabuchi, Y.; Okai, M.; Yamamoto, R.; Tsutsumi, T.; Ono, Y.; Taketsugu, T. SPPR (a developmental version), 2022, Hokkaido University.

(87) Lee, S.; Shostak, S.; Filatov, M.; Choi, C. H. Conical Intersections in Organic Molecules: Benchmarking Mixed-Reference Spin–Flip Time-Dependent DFT (MRSF-TD-DFT) vs Spin–Flip TD-DFT. *J. Phys. Chem. A* **2019**, *123*, 6455–6462.

(88) Ben-Nun, M.; Quenneville, J.; Martínez, T. J. Ab Initio Multiple Spawning: Photochemistry from First Principles Quantum Molecular Dynamics. *Journal of Physical Chemistry A*. 2000, pp 5172–5175.

Table of Contents